Digital Receipt

This receipt acknowledges that Turnitin received your paper. Below you will find the receipt information regarding your submission.

The first page of your submissions is displayed below.

Submission author:	Petrus Sutyasadi
Assignment title:	Petrus Sutyasadi
Submission title:	Industrial Robot
File name:	sutyasadi2020compressed.pdf
File size:	737.16K
Page count:	12
Word count:	6,484
Character count:	32,670
Submission date:	18-Feb-2022 03:20PM (UTC+0700)
Submission ID:	1765313577

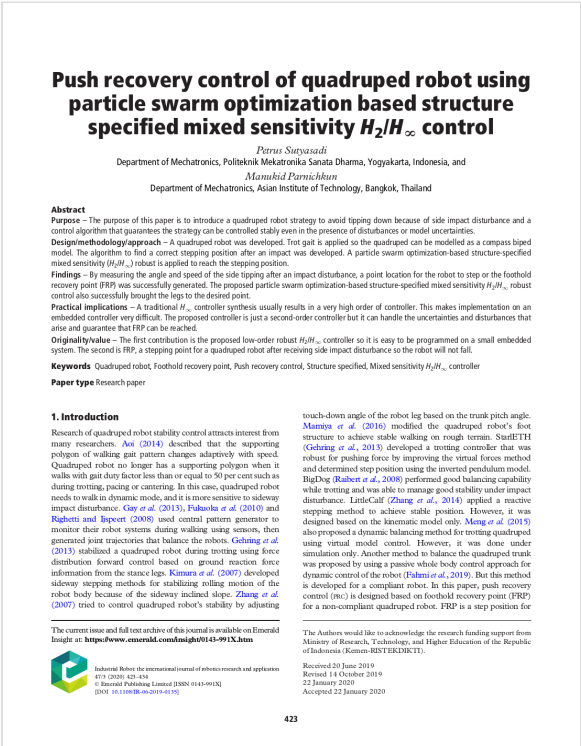

Push recovery control of quadruped robot using particle swarm optimization based structure specified mixed sensitivity H_2/H_∞ control

Petrus Sutyasadi
Department of Mechatronics, Politeknik Mekatronika Sanata Dharma, Yogyakarta, Indonesia, and
Manukid Parnichkun
Department of Mechatronics, Asian Institute of Technology, Bangkok, Thailand

Abstract
Purpose – The purpose of this paper is to introduce a quadruped robot strategy to avoid tipping down because of side impact disturbance and a control algorithm that guarantees the strategy can be controlled stably even in the presence of disturbances or model uncertainties.
Design/methodology/approach – A quadruped robot was developed. Trot gait is applied so the quadruped can be modelled as a compass biped model. The algorithm to find a correct stepping position after an impact was developed. A particle swarm optimization-based structure-specified mixed sensitivity (H_2/H_∞) robust is applied to reach the stepping position.
Findings – By measuring the angle and speed of the side tipping after an impact disturbance, a point location for the robot to step or the foothold recovery point (FRP) was successfully generated. The proposed particle swarm optimization-based structure-specified mixed sensitivity H_2/H_∞ robust control also successfully brought the legs to the desired point.
Practical implications – A traditional H_∞ controller synthesis usually results in a very high order of controller. This makes implementation on an embedded controller very difficult. The proposed controller is just a second-order controller but it can handle the uncertainties and disturbances that arise and guarantee that FRP can be reached.
Originality/value – The first contribution is the proposed low-order robust H_2/H_∞ controller so it is easy to be programmed on a small embedded system. The second is FRP, a stepping point for a quadruped robot after receiving side impact disturbance so the robot will not fall.

Keywords Quadruped robot, Foothold recovery point, Push recovery control, Structure specified, Mixed sensitivity H_2/H_∞ controller

Paper type Research paper

1. Introduction

Research of quadruped robot stability control attracts interest from many researchers. Aoi (2014) described that the supporting polygon of walking gait pattern changes adaptively with speed. Quadruped robot no longer has a supporting polygon when it walks with gait duty factor less than or equal to 50 per cent such as during trotting, pacing or cantering. In this case, quadruped robot needs to walk in dynamic mode, and it is more sensitive to sideway impact disturbance. Guy *et al.* (2013), Fukuoka *et al.* (2010) and Righetti and Ijspeert (2008) used central pattern generator to monitor their robot systems during walking using sensors, then generated joint trajectories that balance the robots. Gehring *et al.* (2013) stabilized a quadruped robot during trotting using force distribution forward control based on ground reaction force information from the stance legs. Kimura *et al.* (2007) developed sideway stepping methods for stabilizing rolling motion of the robot body because of the sideway inclined slope. Zhang *et al.* (2007) tried to control quadruped robot's stability by adjusting touch-down angle of the robot leg based on the trunk pitch angle. Mamiya *et al.* (2016) modified the quadruped robot's foot structure to achieve stable walking on rough terrain. StarlETH (Gehring *et al.*, 2013) developed a trotting controller that was robust for pushing force by improving the virtual forces method and determined step position using the inverted pendulum model. BigDog (Raibert *et al.*, 2008) performed good balancing capability while trotting and was able to manage good stability under impact disturbance. LittleCalf (Zhang *et al.*, 2014) applied a reactive stepping method to achieve stable position. However, it was designed based on the kinematic model only. Meng *et al.* (2015) also proposed a dynamic balancing method for trotting quadruped using virtual model control. However, it was done under simulation only. Another method to balance the quadruped trunk was proposed by using a passive whole body control approach for dynamic control of the robot (Fahmi *et al.*, 2019). But this method is developed for a compliant robot. In this paper, push recovery control (PRC) is designed based on foothold recovery point (FRP) for a non-compliant quadruped robot. FRP is a step position for

The current issue and full text archive of this journal is available on Emerald Insight at: **https://www.emerald.com/insight/0143-991X.htm**

Industrial Robot: the international journal of robotics research and application
47/3 (2020) 423–434
© Emerald Publishing Limited [ISSN 0143-991X]
[DOI 10.1108/IR-06-2019-0135]

The Authors would like to acknowledge the research funding support from Ministry of Research, Technology, and Higher Education of the Republic of Indonesia (Kemen-RISTEKDIKTI).

Received 20 June 2019
Revised 14 October 2019
22 January 2020
Accepted 22 January 2020

Industrial Robot

by Sutyasadi Petrus

Submission date: 18-Feb-2022 03:20PM (UTC+0700)
Submission ID: 1765313577
File name: sutyasadi2020compressed.pdf (737.16K)
Word count: 6484
Character count: 32670

Push recovery control of quadruped robot using particle swarm optimization based structure specified mixed sensitivity H_2/H_∞ control

Petrus Sutyasadi
Department of Mechatronics, Politeknik Mekatronika Sanata Dharma, Yogyakarta, Indonesia, and
Manukid Parnichkun
Department of Mechatronics, Asian Institute of Technology, Bangkok, Thailand

Abstract

Purpose – The purpose of this paper is to introduce a quadruped robot strategy to avoid tipping down because of side impact disturbance and a control algorithm that guarantees the strategy can be controlled stably even in the presence of disturbances or model uncertainties.

Design/methodology/approach – A quadruped robot was developed. Trot gait is applied so the quadruped can be modelled as a compass biped model. The algorithm to find a correct stepping position after an impact was developed. A particle swarm optimization-based structure-specified mixed sensitivity (H_2/H_∞) robust is applied to reach the stepping position.

Findings – By measuring the angle and speed of the side tipping after an impact disturbance, a point location for the robot to step or the foothold recovery point (FRP) was successfully generated. The proposed particle swarm optimization-based structure-specified mixed sensitivity H_2/H_∞ robust control also successfully brought the legs to the desired point.

Practical implications – A traditional H_∞ controller synthesis usually results in a very high order of controller. This makes implementation on an embedded controller very difficult. The proposed controller is just a second-order controller but it can handle the uncertainties and disturbances that arise and guarantee that FRP can be reached.

Originality/value – The first contribution is the proposed low-order robust H_2/H_∞ controller so it is easy to be programmed on a small embedded system. The second is FRP, a stepping point for a quadruped robot after receiving side impact disturbance so the robot will not fall.

Keywords Quadruped robot, Foothold recovery point, Push recovery control, Structure specified, Mixed sensitivity H_2/H_∞ controller

Paper type Research paper

1. Introduction

Research of quadruped robot stability control attracts interest from many researchers. Aoi (2014) described that the supporting polygon of walking gait pattern changes adaptively with speed. Quadruped robot no longer has a supporting polygon when it walks with gait duty factor less than or equal to 50 per cent such as during trotting, pacing or cantering. In this case, quadruped robot needs to walk in dynamic mode, and it is more sensitive to sideway impact disturbance. Gay *et al.* (2013), Fukuoka *et al.* (2010) and Righetti and Ijspeert (2008) used central pattern generator to monitor their robot systems during walking using sensors, then generated joint trajectories that balance the robots. Gehring *et al.* (2013) stabilized a quadruped robot during trotting using force distribution forward control based on ground reaction force information from the stance legs. Kimura *et al.* (2007) developed sideway stepping methods for stabilizing rolling motion of the robot body because of the sideway inclined slope. Zhang *et al.* (2007) tried to control quadruped robot's stability by adjusting touch-down angle of the robot leg based on the trunk pitch angle. Mamiya *et al.* (2016) modified the quadruped robot's foot structure to achieve stable walking on rough terrain. StarlETH (Gehring *et al.*, 2013) developed a trotting controller that was robust for pushing force by improving the virtual forces method and determined step position using the inverted pendulum model. BigDog (Raibert *et al.*, 2008) performed good balancing capability while trotting and was able to manage good stability under impact disturbance. LittleCalf (Zhang *et al.*, 2014) applied a reactive stepping method to achieve stable position. However, it was designed based on the kinematic model only. Meng *et al.* (2015) also proposed a dynamic balancing method for trotting quadruped using virtual model control. However, it was done under simulation only. Another method to balance the quadruped trunk was proposed by using a passive whole body control approach for dynamic control of the robot (Fahmi *et al.*, 2019). But this method is developed for a compliant robot. In this paper, push recovery control (PRC) is designed based on foothold recovery point (FRP) for a non-compliant quadruped robot. FRP is a step position for

The current issue and full text archive of this journal is available on Emerald Insight at: **https://www.emerald.com/insight/0143-991X.htm**

Industrial Robot: the international journal of robotics research and application
47/3 (2020) 423–434

[DOI 10.1108/IR-06-2019-0135]

The Authors would like to acknowledge the research funding support from Ministry of Research, Technology, and Higher Education of the Republic of Indonesia (Kemen-RISTEKDIKTI).

Received 20 June 2019
Revised 14 October 2019
22 January 2020
Accepted 22 January 2020

Industrial Robot: the international journal of robotics research and application
Volume 47 · Number 3 · 2020 · 423–434

reactive step based on the concepts of instantaneous capture points (Pratt and Tedrake, 2005) and orbital energy (Kajita *et al.*, 1990).

H_∞ is a controller that guarantees robust stability under bound uncertainty (Aoi, 2014; Fukuoka *et al.*, 2010; Zhang *et al.*, 2007; Mamiya *et al.*, 2016). However, robust stability obtained from H_∞ alone is not sufficient to achieve robust performance. To solve this problem, H_2/H_∞ optimal control, mixed sensitivity and H_∞ loop shaping were introduced. H_∞ control was applied in many applications (Dzieza and Klempka, 1997; Benderradji *et al.*, 2011; Lu *et al.*, 2016); however, it always resulted in very high order of controller. High-order and complicated structure controller is not desirable in practical. In this research, a simple structure but still retaining the robust stability and robust performance, structure specified mixed sensitivity $H2/H\infty$ controller, is proposed. Particle swarm optimization (PSO), which is a computationally iterative method to optimize nonlinear system (Kennedy and Ebenhart, 1995), is used to search for the optimal parameters of the controller that satisfy robust stability, robust performance and small tracking error cost function criterion. The objective of selecting mixed sensitivity $H2/H\infty$ controller is to robustly track the quadruped's leg joints angle. Therefore, even in the presence of uncertainties, the swinging legs of the quadruped can reach the FRP properly and prevent the robot from falling sideways.

2. Hardware design of AIT quadruped

Specification of Asian Institute of Technology (AIT) quadruped robot is provided in Table I. It has total of 12 degrees of freedom (DoF) with 3 DoF on each leg. Details of the robot and its mechanical design are shown in Figure 1.

The robot has two levels of controller. The low-level controller is used to control joint angle of the legs, whereas the gait pattern generation, the balancing control and the PRC are controlled by the high-level controller. The details of the schematic diagram are shown in Figure 2 (Sutyasadi and Parnichkun, 2016).

3. Kinematic of AIT quadruped robot

Reference coordinate systems are embedded on each leg of AIT quadruped robot as shown in Figure 3. Based on the embedded reference coordinate systems, the Denavit Hartenberg (D-H) parameters are given in Table II.

The joint angles θ_1, θ_2 and θ_3 are derived from the known foot position (x,y,z).

Table I Hardware specification of AIT quadruped robot

Specification	Value
Length	400 mm
Width	281 mm
Height	285 mm
Weight	10.25 kg
Battery	12V × 2
Degree of freedom	12DoF
DC Motor power	18W × 8, 25W × 4

Source: Sutyasadi and Parnichkun (2016)

Figure 1 (a) AIT quadruped robot and (b) mechanical design of AIT quadruped robot

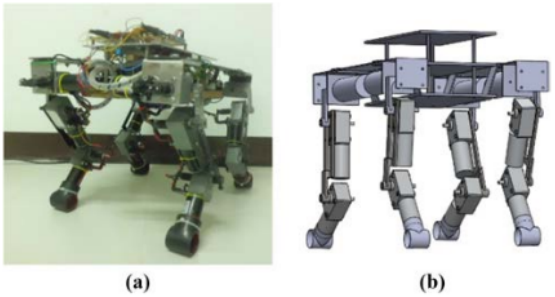

(a) (b)

$$\theta_1 = a\tan\left(\frac{y}{x}\right) \tag{1}$$

$$\theta_2 = -a\tan\frac{B}{A} + a\tan\left(\frac{D}{\pm\sqrt{r^2 - D^2}}\right) \tag{2}$$

$$\theta_3 = a\tan\left(\frac{z - a_2\sin\theta_2}{x\cos\theta_1 + y\sin\theta_1 - a_2\cos\theta_2 - a_1) - \theta_2}\right) \tag{3}$$

where,

$$A = -z \tag{4}$$

$$B = a_1 - (x\cos\theta_1 + y\sin\theta_1) \tag{5}$$

$$D = \frac{2a_1(x\cos\theta_1 + y\sin\theta_1) + a_3^2 - a_2^{22}}{2a_2} + \frac{-a_1^2 - z^2 - (x\cos\theta_1 + y\sin\theta_1)^2}{2a_2} \tag{6}$$

4. Push recovery control

In this research, foot recovery point (FRP), or the stepping position of the swinging foot for the recovery because of the sideway impact disturbance and structure specified mixed sensitivity $H2/H\infty$ controller, is proposed for the quadruped robot. A trotting quadruped can be modelled as a biped (Polet and Bertram, 2019; Gan *et al.*, 2018; Ugurlu *et al.*, 2013). When a quadruped walks in a trot gait, its feet can be paired diagonally as shown in Figure 4. During the trot gait, the quadruped is only supported by one pair of diagonal stance legs that move simultaneously. The two pairs of the legs swing alternately as a biped moves using its two legs. Each of the quadruped's diagonal legs pair represent one of the biped legs. When one of the diagonal legs pair swings, the other pair is in stance position just like a biped walks. The left foot of the biped is the middle point between front left and rear right pair of the quadruped legs. The right foot of the biped is the middle point between front right and rear left pair of the quadruped legs.

Industrial Robot: the international journal of robotics research and application
Volume 47 · Number 3 · 2020 · 423–434

Figure 2 Schematic diagram of the controllers of the quadruped robot

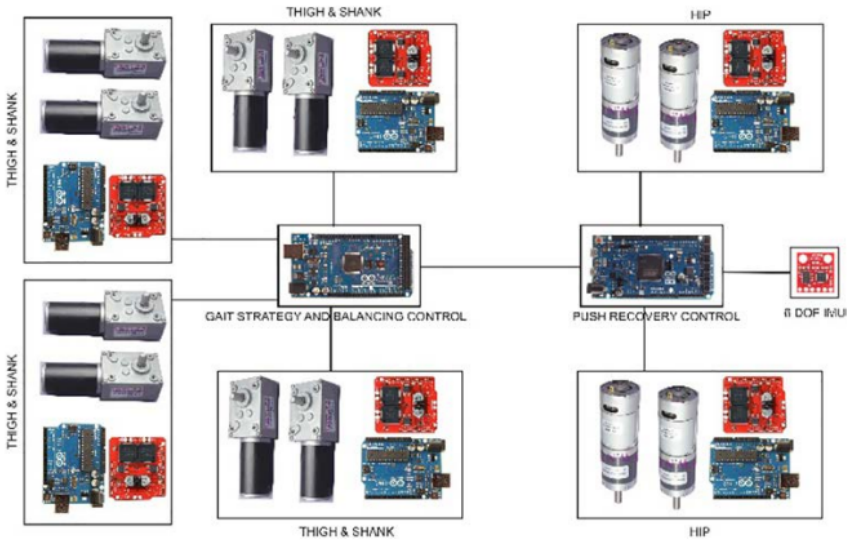

Figure 3 Reference coordinate systems on each leg of AIT quadruped robot

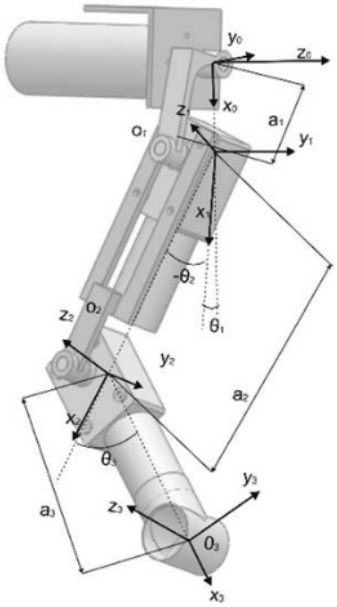

Table II D-H Parameters of AIT quadruped robot

Parameter	Link 1	Link 2	Link 3
a_i	a_1	a_2	a_3
α_i	$\pi/2$	0	0
d_i	0	0	0
θ_i	θ_1	θ_2	θ_3

4.1 Foothold recovery point

The quadruped robot falls either to the left or to the right if a disturbance force with significant amplitude is applied. The swinging legs should step to a correct position to avoid falling. This particular stepping position is called FRP. Figure 5 shows that to simplify the model, the falling of the quadruped was modelled into compass biped movement. The swinging quadruped legs of the other pair was calculated based on the compass biped model.

In the compass biped robot model, the FRP position is determined by using the law of conservation of angular momentum. The robot's configuration from the moment when a disturbance force is applied until the robot's final position is shown in Figure 6. The notation of θ_a, θ_b, l_A and l_B shown in Figure 5 shows the parameters that represent the angle and the length of the leg when modelled as a biped. Figure 6 shows the parameters in a planar model when the biped tilted and swung the other legs to the FRP point.

Target position is shown in Figure 6(c), where:

$$\theta_c = 0 \quad \text{and} \quad \dot{\theta}_c = 0 \tag{7}$$

Based on the angular motion equation,

$$\frac{\omega_1^2 - \omega_0^2}{2\theta} = \alpha \tag{8}$$

Angular acceleration of the swinging leg is determined from:

$$\frac{\dot{\theta}_C^2 - \dot{\theta}_B^2}{2\theta_B} = \ddot{\theta}_B \tag{9}$$

When the foot strikes the ground, there is an energy loss and discontinuity of motion because of the impact. The quadruped feet are made so that they have sufficient friction

Figure 4 Foot configuration and representation of quadruped trotting gait as biped walking gait

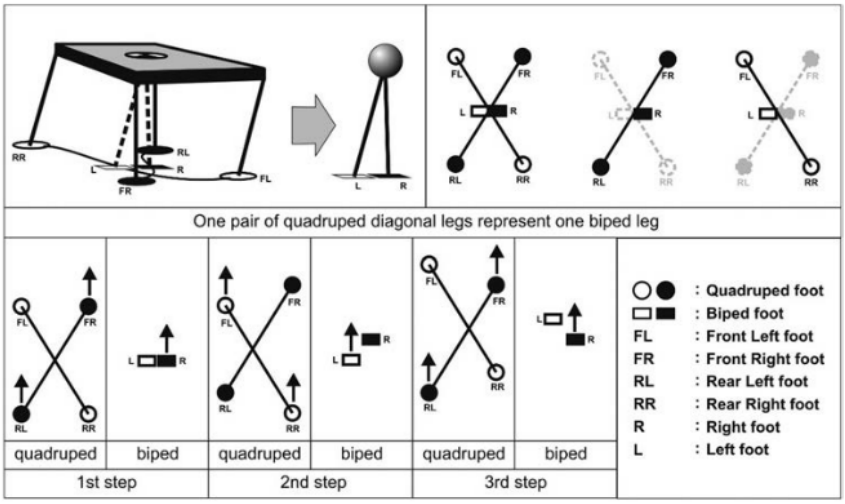

Figure 5 Falling quadruped modelled as compass biped

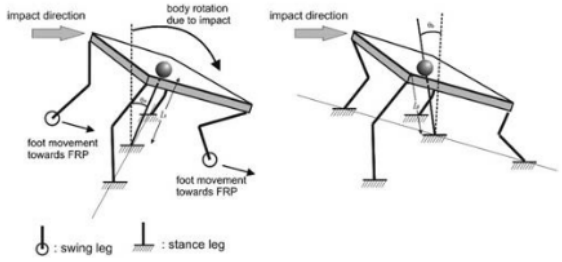

Figure 6 PRC using FRP (a) initial position, (b) leaning sideway pivoting on the first leg (Ia) and the other leg (Ib) swings and (c) final position

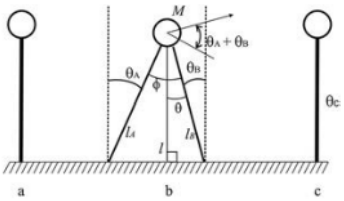

to prevent slips at the contact points. Thus, the conservation of angular momentum around the contact point is assumed as:

$$I^{+}\omega^{+} = I^{-}\omega^{-} \tag{10}$$

where "+" and "−" denote post- and pre-impact, respectively.

According to Garcia *et al.* (1998), the relation between post- and pre-impact angular position and velocity is expressed in the following equation:

$$\begin{bmatrix}\theta\\ \dot{\theta}\end{bmatrix}^{+} = \begin{bmatrix}-1 & 0\\ 0 & \cos 2\theta\end{bmatrix}\begin{bmatrix}\theta\\ \dot{\theta}\end{bmatrix}^{-} \tag{11}$$

The relation of angular velocity before and after impact has been widely used in compass biped robot researches and presented for the first time by Mc Geer (1990). In the compass biped robot, there is a rule that the collision/impact occurs when (Garcia *et al.*, 1998):

$$\phi(t) - 2\theta(t) = 0 \tag{12}$$

Where, θ is the angle between the stance leg and the surface normal and ϕ is the angle between the stance leg and the swinging leg. The details of ϕ and θ can be seen in Figure 6(b).

In the quadruped robot model, the angle between the stance leg and the swinging leg is $\phi = \theta_A + \theta_B$. Therefore, instead of using cos 2θ for determining the post-impact angular velocity as proposed by Garcia *et al.* (1998), $\cos(\theta_A + \theta_B)$ is used instead. By the conservation of angular momentum (Mc Geer, 1990):

$$ml_B^2\omega^{+} = ml_A^2\omega^{-}\cos(\theta_A + \theta_B) \tag{13}$$

where $\omega^{+} = \dot{\theta}_B$ is the final angular velocity and $\omega^{-} = \dot{\theta}_A$ is the initial angular velocity. Therefore, the post-impact angular velocity as a function of pre-impact angular velocity is expressed by:

$$\dot{\theta}_B = \frac{ml_A^2\dot{\theta}_A\cos(\theta_A + \theta_B)}{ml_B^2} \tag{14}$$

$$\dot{\theta}_B = \frac{ml_A^2\dot{\theta}_A(\cos\theta_A\cos\theta_B - \sin\theta_A\sin\theta_B)}{ml_B^2} \tag{15}$$

At the last rotation of the body around pivot point on l_B,

$$ml_B^2\ddot{\theta}_B = mgl_B\theta_B \tag{16}$$

$$\ddot{\theta}_B = \frac{g\theta_B}{l_B} \tag{17}$$

From equations (7), (9) and (17):

$$\frac{-\dot{\theta}_B^2}{2\theta_B} = \frac{g\theta_B}{l_B} \tag{18}$$

$$\dot{\theta}_B = -\sqrt{\frac{2g}{l_B}}\theta_B \tag{19}$$

From equations (15) and (19):

$$-\sqrt{\frac{2g}{l_B}}\theta_B = \frac{ml_A^2\dot{\theta}_A\left(\cos\theta_A\left(1-\frac{\theta_B^2}{2}\right)-\sin\theta_A\theta_B\right)}{ml_B^2} \tag{20}$$

$$-l_B^2\sqrt{\frac{2g}{l_B}}\theta_B = l_A^2\dot{\theta}_A\left(2\cos\theta_A - cos\theta_A\theta_B^2 - 2\sin\theta_A\theta_B\right) \tag{21}$$

$$-\frac{l_B^2}{l_A^2\dot{\theta}_A}\sqrt{\frac{2g}{l_B}}\theta_B = \left(2\cos\theta_A - cos\theta_A\theta_B^2 - 2\sin\theta_A\theta_B\right) \tag{22}$$

$$cos\theta_A\theta_B^2 - \left(\frac{l_B^2}{l_A^2\dot{\theta}_A}\sqrt{\frac{2g}{l_B}} + 2\sin\theta_A\right)\theta_B - 2\cos\theta_A = 0 \tag{23}$$

By applying small angle approximation, thus $l_B \approx l$ where l is the center of mass height, hence,

$$l_B = l_A\cos\theta_A \tag{24}$$

Solving θ_B from (23) and l_B from (24) results in FRP position that makes the quadruped robot achieve its stable position in one step of recovery movement. In the real implementation, l_B of the compass biped robot is transformed into the quadruped robot's leg equivalent length. If the quadruped trots in normal condition, all the hip heights are the same. When the quadruped is falling, then the height of the four corners of the quadruped body are not the same. Figure 7 shows the detail of the situation and the length difference of the legs during the recovery.

The lower hip height of the robot is as follows:

$$l_s = l_B\cos\theta_B - a\sin(90-\varphi_r) \tag{25}$$

Whereas, the higher hip height of the robot is as follows:

$$l_h = l_B\cos\theta_B + a\sin(90-\varphi_r) \tag{26}$$

where,

l_s = lower hip height;
l_h = higher hip height;

Figure 7 Hip heights of two swinging legs during trotting

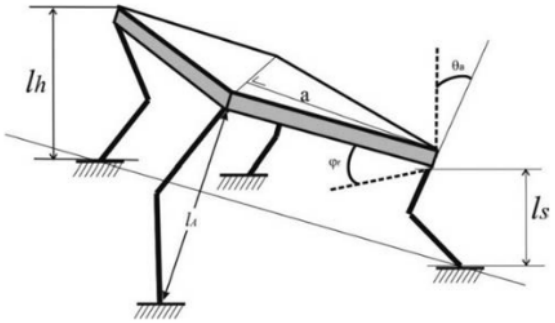

φ_r = trunk roll angle; and
a = perpendicular distance from swing hip to diagonal line connecting stance hips.

4.2 Structure specified mixed sensitivity H_2/H_∞ controller

The quadruped robot model is a highly non-linear and coupled dynamic model. The model is linearized by using feedback linearization so that a linear robust controller can be applied (Lewis *et al.*, 1993).

The linearization is conducted using the feedback linearization method. The quadruped robot is modeled as a compass biped robot model:

$$M(\theta).\ddot{\theta} + C(\theta,\dot{\theta}).\dot{\theta} + G(\theta) = \tau \tag{27}$$

The mass, coriolis and gravity matrices of the compass biped robot are expressed by:

$$M = \begin{bmatrix} m_hl^2 + m(l^2+a^2+b^2-2bl\cos\theta_b) & mb(b-l\cos\theta_b) \\ mb(b-l\cos\theta_b) & mb^2 \end{bmatrix}$$
$$C = \begin{bmatrix} 2mbl(\sin\theta_b)\dot{\theta}_b & mbl(\sin\theta_b)\dot{\theta}_b \\ -mbl(\sin\theta_b)\dot{\theta}_a & 0 \end{bmatrix}$$
$$G = \begin{bmatrix} -g(ma+ml+m_hl)\sin\theta_a + mb\sin(\theta_a+\theta_b) \\ gmb\sin(\theta_a+\theta_b) \end{bmatrix} \tag{28}$$

where, τ is the joint torque, m_h is mass of the point mass biped robot, m is leg mass, l is leg length with the value of a and b for the upper and lower segments, respectively, θ_a and θ_b are legs angular positions, respectively and g is the earth gravity.

A 2-DOF compass biped robot consists of two legs driven by 2 DC motors. Dynamic model of a DC motor is expressed in the following equation:

$$\mathcal{J}\ddot{\theta} + b\dot{\theta} = Ki \tag{29}$$

$$L\frac{di}{dt} + Ri = V - K\dot{\theta} \tag{30}$$

where $\mathcal{J}$ is the inertia of the motor, b is viscous friction constant, i is the armature current, L is the electric inductance, R is the

armature resistance, V is the voltage source and θ is the angle of the rotor position. The electromotive force constant and the motor torque constant are equal and symbolized with K.

The state-space equation of the motor and the connected link is represented by:

$$\frac{d}{dt}\begin{bmatrix}\theta\\ \dot{\theta}\\ i\end{bmatrix}=\begin{bmatrix}0 & 1 & 0\\ 0 & -\frac{b}{\mathcal{J}} & \frac{K}{\mathcal{J}}\\ 0 & -\frac{K}{L} & -\frac{R}{L}\end{bmatrix}\begin{bmatrix}\theta\\ \dot{\theta}\\ i\end{bmatrix}+\begin{bmatrix}0\\ 0\\ \frac{1}{L}\end{bmatrix}V \qquad (31)$$

$$y=\begin{bmatrix}1 & 0 & 0\end{bmatrix}\begin{bmatrix}\theta\\ \dot{\theta}\\ i\end{bmatrix}$$

After substitution of the parameters, the matrices A and B become:

$$A=\begin{bmatrix}0 & 1 & 0\\ 0 & -0.7011 & 7.5367\text{exp}+03\\ 0 & -8.9883\text{exp}+03 & -1.1924\text{exp}+06\end{bmatrix}$$

$$B=\begin{bmatrix}0\\ 0\\ 3.1987\text{exp}+05\end{bmatrix} \qquad (32)$$

Input of the system is voltage (V) and output is angular position of the leg joint angle (θ). The transfer function of the system becomes:

$$\frac{\Theta(s)}{V(s)}=\frac{0.0281}{1.166\text{exp}-11\,s^3+1.39\text{exp}-05\,s^2+0.0007994\,s} \qquad (33)$$

If a controller, $K(s)$ is designed so that the closed loop of the nominal system is asymptotically stable, robust stability performance against external disturbance satisfies the following inequality:

$$\mathcal{J}_{\infty,a}=\|W_s(s)S(s)\|_\infty<1 \qquad (34)$$

A stable function $W_s(s)$ is used to attenuate external disturbances. The multiplicative perturbation is upper bounded by another stable function $W_t(s)$. The robust stability against system perturbation satisfies the following inequality:

$$\mathcal{J}_{\infty,b}=\|W_t(s)T(s)\|_\infty<1 \qquad (35)$$

where, W_s is sensitivity weight, $W_t(s)$ is complementary sensitivity weight, $S(s)$ is the sensitivity function and $T(s)$ is the complementary sensitivity or transmissibility function. The purpose of the design of structure specified mixed sensitivity H_2/H_∞ control is to find an admissible structure-specified controller that minimizes the cost function $\mathcal{J}_2$ subjected to both constraints of $\mathcal{J}_{\infty,a}$ and $\mathcal{J}_{\infty,b}$.

$$\mathcal{J}_2=\int_0^\infty e^2(t)dt=\|E(s)\|_2^2 \qquad (36)$$

4.2.1 Weights selection

Consider loop transfer (L), sensitivity function (S) and complementary sensitivity function (T) with controller (K) and plant (G) of the system as shown by the block diagram in Figure 8.

$$L(s)=K(s).G(s) \qquad (37)$$

$$S(s)=\frac{1}{1+K(s).G(s)} \qquad (38)$$

$$T(s)=\frac{K(s).G(s)}{1+K(s).G(s)} \qquad (39)$$

Model uncertainties can be modeled as multiplicative perturbation (Wei-Gu *et al.*, 2013). Block diagram of the system is shown in Figure 9.

If $r(s)$, $d(s)$ and $n(s)$ are assumed zero to consider only the effect of uncertainties, the transfer function from $v(s)$ to $w(s)$ of the system shown in Figure 9 becomes:

$$\frac{w(s)}{v(s)}=\frac{-K(s).G(s)}{I+K(s).G(s)} \qquad (40)$$

To reduce the effect of uncertainties, the complementary sensitivity function should be small, ≈ 0.

It is not possible to make the sensitivity function, S, and complementary sensitivity function, T, become small at the same time since $S+T=I$. Thus, a trade-off between S and T is required.

4.2.2 Sensitivity weight selection

The weights are used to normalize the input and output to one. Therefore, if Ws is the sensitivity weight, then the magnitude of WsS is less than or equal to 1 over all frequencies. Thus, the inverse of Ws becomes the upper bound and shapes the

Figure 8 Block diagram of a closed loop control system

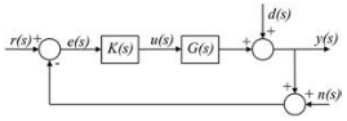

Figure 9 Closed loop system with multiplicative uncertainties

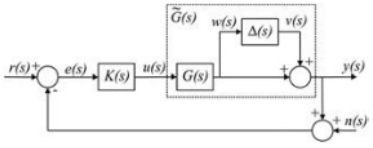

Industrial Robot: the international journal of robotics research and application
Volume 47 · Number 3 · 2020 · 423–434

Figure 10 Sensitivity and its weight singular plot

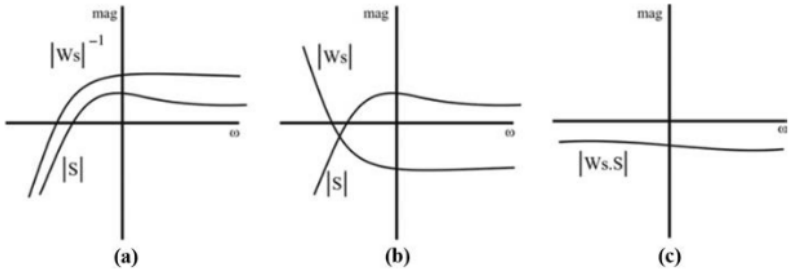

sensitivity function. Figure 10 shows the relationship between the weight, Ws and sensitivity function, S.

The sensitivity weight function is selected using Skogestad's method (Skogestad, 2001).

$$W_s(s) = \frac{s/M + \omega_B}{s + \omega_B.A} \tag{41}$$

where, M is the sensitivity peak used to limit the overshoot, $A < 1$ is the minimum steady-state offset and ω_B is the desired bandwidth. Selecting $A \ll 1$ causes the result resemble to integral action (Skogestad, 2001). A large value of ω_B causes fast response. The maximum peak of $|S|$ is less than M. In the quadruped robot, the sensitivity weight for the FRP is selected as:

$$W_s(s) = \frac{0.5s + 1}{s + 0.001} \tag{42}$$

The inverse of the sensitivity weight singular value is shown in Figure 11.

4.2.3 Complementary sensitivity weight selection

For the output multiplicative perturbation problem, the complementary sensitivity weight relates with the uncertainties, according to Wei-Gu *et al.* (2013) and Skogestad (2001), by:

Figure 11 The inverse of the sensitivity weight singular value

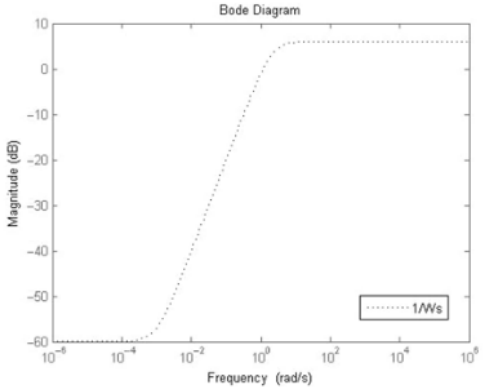

$$\left\| \frac{G(s).K(s)}{I + G(s).K(s)} \right\|_\infty < \frac{1}{\|\Delta\|_\infty} \tag{43}$$

The complementary sensitivity weight function, Wt, is the upper bound of the maximum possible uncertainties. Thus, the inequality equation (43) becomes:

$$\left\| \frac{G(s).K(s)}{I + G(s).K(s)} \right\|_\infty < \frac{1}{\|W_t\|_\infty} \tag{44}$$

The steps to select the complementary sensitivity weight function for multiplicative perturbation problem are as follows:

- plot singular value of all uncertainties $\Delta(j\omega)$; and
- upper bound the uncertainties by the weight function Wt.

Based on the multiplicative perturbation and the nominal system, all the uncertainties and the upper bound weight are determined and plotted as shown in equation (45) and Figure 12.

$$W_t(s) = \frac{3.428s^2 + 5.569s + 2.793}{s^2 + 172.9s + 243.2} \tag{45}$$

In structure specified mixed sensitivity H_2/H_∞ controller for the quadruped robot, the proportional integral derivative structure with filtered derivative is selected as expressed by:

Figure 12 The complementary sensitivity and system uncertainties singular values

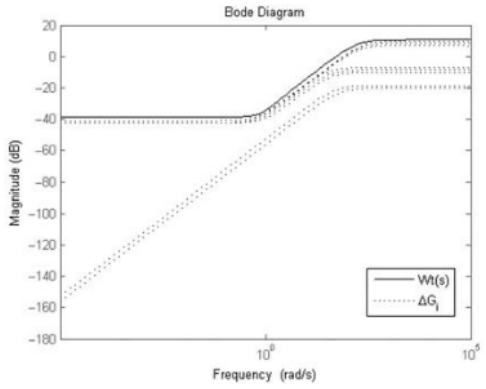

Figure 13 Flowchart of PSO

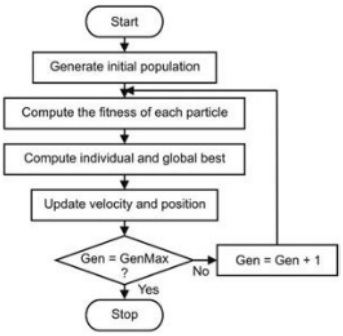

$$K(s) = Kp + \frac{Ki}{s} + \frac{Kd.s}{Td.s + 1} \tag{46}$$

PSO is applied to determine the optimal values of the controller gains and parameters such as K_p, K_i, K_d, and T_d.

4.3 Particle swarm optimization

PSO is an evolutional method used to optimize a wide range of objective function by adopting a social behavior like the behavior of flocking birds or school of fish (Kennedy and Eberhart, 1995). Flow chart of PSO is depicted in Figure 13. $x_i = (x_{i1}, x_{i2}, \ldots, x_{iN})$ is position vector of particle, $v_i = (v_{i1}, v_{i2}, \ldots, v_{iN})$ is velocity vector of particle, $p_i = (p_{i1}, p_{i2}, \ldots, p_{iN})$ is the best previous position of particle i.

Global best position is the best individual position of the whole swarm $G = (g_1, g_2, \ldots, g_N)$. The velocity and the position of the particle are updated every iteration:

$$v_i(k+1) = w.v_i(k) + c_1.r_1.(P_i(k) - x_i(k)) + c_2.r_2.(G(k) - x_i(k)) \tag{47}$$

$$x_i(k+1) = x_i(k) + v_i(k) \tag{48}$$

where, w is inertia weight, r_1 and r_2 are random variables ranged between 0 to 1, c_1 and c_2 are coefficients of acceleration. The velocity is kept in the range of $-v_{min}$ to v_{max}.

5. Simulation result

The parameters of the PSO are set as follows: swarm size = 20, dimension of the particle is 4 (kp, ki, kd and td), $c_1 = c_2 = 2$ and number of maximum generation = 100. The inertia weight is changed from 0.95 to the final weight 0.4, and the velocity is limited at $[-v_{min}, v_{max}] = [-100, 100]$.

The result is obtained as:

$$K(s) = 1.76493 + \frac{0.80362}{s} + \frac{0.26895.s}{0.00016s + 1} \tag{49}$$

With the $\gamma_{\infty,a} = 0.5028$, $\gamma_{\infty,b} = 0.6354$ and $\gamma_2 = 0.0128$.

Figure 14 shows that inverse of the weight functions is larger than the sensitivity function and the complementary sensitivity function which confirms $|WsS| < 1$ and $|WtT| < 1$.

Figure 14 The sensitivity, complementary sensitivity and their inverse weights singular values using proposed controller

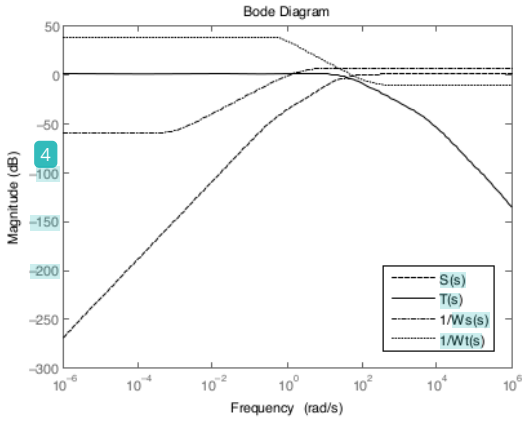

Figure 15 shows that PSO-based structure-specified mixed sensitivity H_2/H_∞ controller is able to control the quadruped robot even under various uncertainties. Small overshoot for a short period when the swinging leg is still in flight phase is seen. There is no steady state error. The response has satisfactory rise time and settling time even under uncertainties. The results show that all the system responses have settling time less than 0.6 s. Half of them have less than 0.4 s settling time.

A well-tuned proportional derivative controller is implemented for comparison purpose. Figure 16 shows the performance of PD controller under the same uncertainties.

The result shows that the well-tuned PD controller performs very well without overshoot and short settling time on the nominal system. It has settling time around 0.4 s (black color). However, with the maximum uncertainty (light blue dashed), the system response has settling time more than 1 s. Most responses show almost 1-s settling time.

The proportional gain is then increased to get a faster response. The results show that the settling time on the maximum

Figure 15 PSO-based structure-specified mixed sensitivity H_2/H_∞ controller performances under inertia and armature resistance uncertainties (nom: nominal, min: minimum, max: maximum).

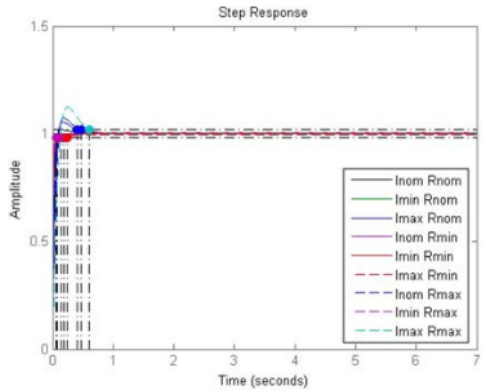

Figure 16 PD controller performances under uncertainties

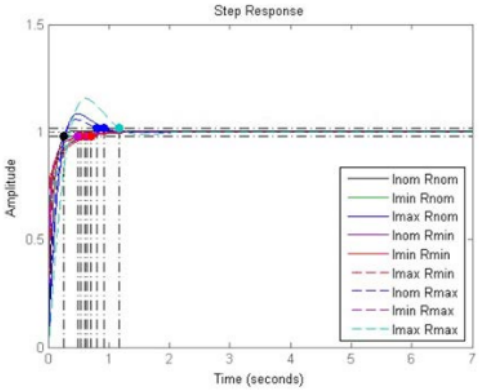

uncertainty increases compared with the previous gain and overshoot increases in some responses as shown in Figure 17.

The well-tuned PD controller shows good performance for the nominal system. However, it performs worse than PSO-based structure-specified mixed sensitivity H_2/H_∞ controller under uncertainties.

To compare the performance of the proposed PSO-based structure-specified mixed sensitivity H_2/H_∞ controller with full-order mixed sensitivity H_∞ controller using the same plant, sensitivity weight and complementary sensitivity weight, full-order mixed sensitivity H_∞ controller is determined and obtained as shown in equation (52).

Figure 18 shows that singular plot of the sensitivity, complementary sensitivity and their weights using the full-order controller also satisfy the requirement.

With the same uncertainties, full-order mixed sensitivity H_∞ controller is tested using step function similar to PD and the proposed controller. The simulation results of the system response using full-order mixed sensitivity H_∞ controller is shown in Figure 19.

It is shown that the system response using full-order mixed sensitivity H_∞ controller has no steady state error. However,

Figure 17 PD controller performances under uncertainties with higher proportional gain

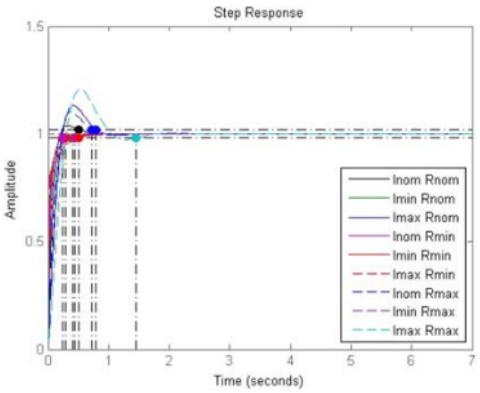

Figure 18 The sensitivity, complementary sensitivity and their inverse weights singular values using full-order controller

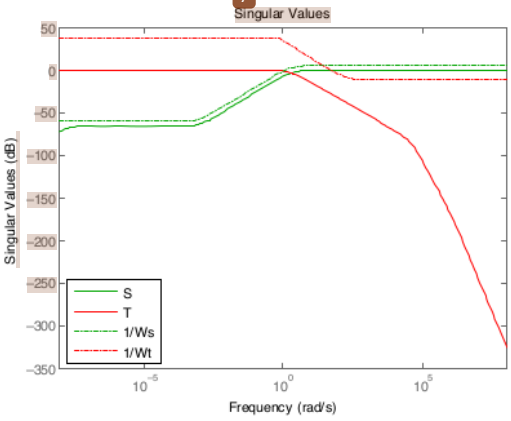

Figure 19 Full-order controller performances under uncertainties

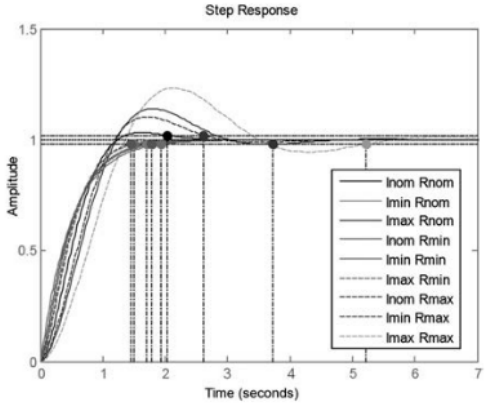

the settling times of the response are too long. Compared with the proposed controller and the well-tuned PD controller, full-order mixed sensitivity H_∞ robust controller provides more overshoot. Basically, all of the responses are stable under the uncertainties, but the system responses are worse. In conclusion, under uncertainties, PSO-based structure-specified mixed sensitivity H_2/H_∞ controller has better performance than PD controller and full-order mixed sensitivity H_∞ controller.

$$K(s) = \frac{2.076e06s^5 + 2.475e12s^4 + 5.702e14s^3 + 2.521e16s^2 + 3.461e16s + 1.897e06}{s^6 + 1.249e06s^5 + 6.951e10s^4 + 1.935e15s^3 + 4.323e17s^2 + 6.092e17s + 6.085e14} \quad (50)$$

6. Experimental result

Experiments are conducted by using several initial foot positions and the desired FRP targets. The FRP target position is defined at 30° of FRP angle (θ_B) and the FRP length (l_B) is the same as the initial position length.

Industrial Robot: the international journal of robotics research and application
Volume 47 · Number 3 · 2020 · 423–434

Figure 20 shows step responses of the system using PSO-based structure-specified mixed sensitivity H_2/H_∞ controller under uncertainties. Six experiments with different leg orientations are conducted. The results show that overshoots appear in all responses. However, the settling time of all the responses is less than 0.5 s. The overshoot occurs while the leg is still swinging in the air. The biggest overshoot occurs when the impact disturbance is applied when the leg is in the maximum stretch position which results in the largest moment. At the minimum stretch position or maximum swing height, the leg has the minimum moment. At this position, the response also has overshoot. The results show that the responses from PSO-based structure-specified mixed sensitivity H_2/H_∞ controller are not much different under model uncertainties.

Figure 21 shows step responses of the system controlled by well-tuned PD controller. The system has overshoot when the leg position is in the maximum stretch. However, the overshoot is smaller compared with the results obtained from PSO-based structure-specified mixed sensitivity $H2/H\infty$ controller. When the leg is in the minimum stretch position or in the maximum swing height, the system response does not have an overshoot but a steady state error exists. When the leg is not at the maximum or minimum stretch, the response also has an overshoot and a steady state error also exists. The experimental results show that the steady state error varies drastically during

Figure 20 System responses under uncertainties controlled by PSO-based structure-specified mixed sensitivity H_2/H_∞ controller

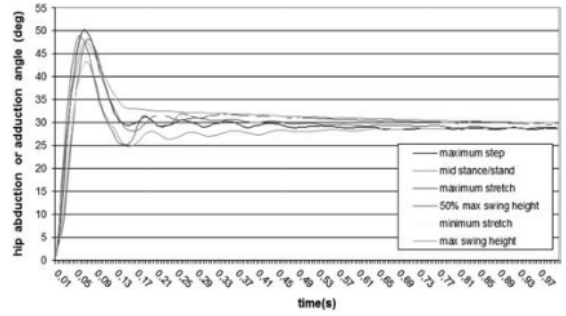

Figure 21 System responses under uncertainties controlled by PD controller

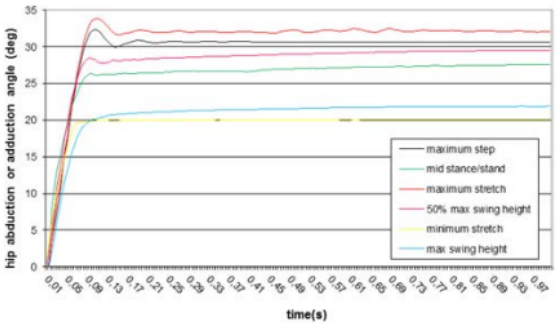

the experiments. The results show that PD controller is more sensitive to model uncertainty compared with PSO-based structure-specified mixed sensitivity $H2/H\infty$ controller.

Figure 22 shows the trunk roll angle when the quadruped robot trots and an impact disturbance is applied. The robot can continue trotting without fall. Before applying the impact disturbance, the robot has a small trunk roll angle variation around $\pm 1.5°$. After the impact, the quadruped robot has around $+5$ to $-17°$ of trunk roll angle during the recovery. The maximum or minimum roll angle indicates the trunk position when the swinging or the recovery legs land on the ground before the other diagonal pair of the legs swing to align the body. Small oscillation starting after 3.5 s indicates that the robot continues to trot after conducting a recovery step. One cycle of recovery process takes around 2 s until the robot is able to continue trotting again.

Figure 23 shows that without the FRP, the quadruped robot has no reflect to swing its leg sideways to balance the body when an impact force applied to the robot. Figure 23(a) shows the quadruped trotting forward. When the sideways force came, the robot had only trot command in its controller. Moreover, the leg was designed to have zero or very less friction between the shoe and the floor. Therefore, when the sideways disturbance came, the foot on the other side of the coming impact stuck on the floor, and the robot tilted on the direction of the impact [Figure 23(b)]. The sideways force was so big the

Figure 22 Trunk roll angle during push recovery process.

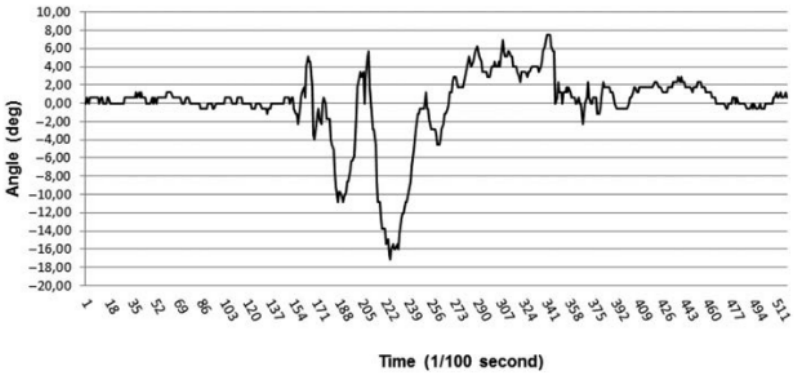

Figure 23 Snap shot images from video movie experiment of side impact disturbance applied to trotting quadruped robot without FRP algorithm

Figure 24 Snap shot images from video movie experiment of side impact disturbance applied to trotting quadruped robot, with foot recovery algorithm implemented on the quadruped controller

swinging mass was made from books put on a carton box, which weighed around 20 Kgs. It was enough to push the robot to continue falling sideways [Figure 23(c)-(d)], until it completely fell down in Figure 23(e) and 23(f).

Figure 24 shows some snap shot images from the video movie of experiment when the quadruped controller is added with the push recovery algorithm. Figure 24(a) and 24(b) show the quadruped robot trotting before the impact. Figure 24(c) shows the swinging leg position just before the impact. After the impact disturbance occurs, the swinging legs swing sideways to reach the stepping point [Figure 24(d)]. Once the legs land [Figure 24(e)], the other pair of the legs swing to align the robot following the momentum from the impact disturbance. Figure 24(f) shows the quadruped robot is ready to continue the trot.

7. Conclusion

Dynamic walking was implemented via a trotting gait pattern. The quadruped robot could move forward, walk in place, rotate to the right and left during trotting. The proposed FRP worked effectively and provided fast recovery with single step. To reach FRP, PSO-based structure-specified mixed sensitivity $H2/H\infty$ controller was proposed to handle the uncertainties. It performed better than the well-tuned PD controller. The robot was able to stabilize itself when impact disturbance was applied to the system using the proposed PRC. Both feet could be positioned using FRP as seen from simulations and experiments with the settling time less than 0.8 s. Furthermore, the recovery process using PRC required less than 2 s to recover from the maximum trunk leaning angle after the impact disturbance to its initial (desired) trunk angle. The results also showed that the proposed controller was robust to uncertainty from parameters variation. The FRP was designed for non-compliant robot. The correct stepping position to the FRP will prevent hard impact between the foot and the floor. Future study should also consider the whole dynamics of the body for compliant robot mechanism.

References

Aoi, S. (2014), "Simple legged robots that reveal biomechanical and neuromechanical functions in locomotion dynamics", *Journal of Robotics and Mechatronics*, Vol. 26 No. 1, pp. 98-99.

Benderradji, H. Chrifi-Alaoui, , L. and Makouf, A. (2011), "H∞ control using sliding mode linearization technique applied to an induction motor", s.l., s.n., pp. 1-6.

Dzieza, J. and Klempka, R. (1997), "H∞ control of DC motors", s.l., s.n., pp. 137-142.

Fahmi, S., Mastalli, C., Focchi, M. and Semini, C. (2019), "Passive whole-body control for quadruped robots: experimental validation over challenging terrain", *IEEE Robotics and Automation Letters*.

Fukuoka, Y., Katabuchi, H. and Kimura, H. (2010), "Dynamic locomotion of quadrupeds tekken 3&4 using simple navigation", *Journal of Robotics and Mechatronics*, Vol. 22 No. 1, pp. 36-42.

Gan, Z., Jiao, Z. and Remy, C.D. (2018), "On the dynamic similarity between bipeds and quadrupeds: a case study on bounding", *IEEE Robotics and Automation Letters*, Vol. 3 No. 4, pp. 3614-3621.

Garcia, M., Chatterjee, A., Ruina, A. and Coleman, M. (1998), "The simplest walking model: stability, complexity, and scaling", *Journal of Biomechanical Engineering*, Vol. 120 No. 2, pp. 281-288.

Gay, S. Santos-Victor, J. and Ijspeert, A. (2013), "Learning robot gait stability using neural networks as sensory feedback function for Central pattern generators", Tokyo, pp. 194-201.

Gehring, C. Coros, S. and Marco Hutter, M. (2013), "Control of dynamic gaits for a quadrupedal robot", s.l., s.n., pp. 3287-3329.

Kajita, S. Tani, K. and Kobayashi, A. (1990), "Dynamic walk control of a biped robot along the potential energy conserving orbit", p. 789 -794.

Kennedy, J. and Ebenhart, R. (1995), "Particle swarm optimization", s.l., s.n., pp. 1942-1948.

Kimura, H., Fukuoka, Y. and Cohen, A. (2007), "Adaptive dynamic walking of a quadruped robot on natural ground based on biological concepts", *The International Journal of Robotics Research*, Vol. 26 No. 5, pp. 475-490.

Lewis, F.L., Dawson, D.M. and Abdallah, C.T. (1993), *Robot Manipulator Control: Theory and Practice*, Prentice Hall, New York, NY.

Lu, Q., Sorniotti, A., Gruber, P. and Theusnissen, J. (2016), "H∞ loop shaping for the torque-vectoring control of electric vehicles: theoretical design and experimental assessment", *Mechatronics*, Vol. 35, pp. 32-43.

Mc Geer, T. (1990), "Passive dynamic walking", *International Journal of Robotic Research*, Vol. 9, pp. 62-82.

Mamiya, S., Sano, S. and Uchiyama, N. (2016), "Foot structure with divided flat soles and springs for legged robot and experimental verification", *Journal of Robotics and Mechatronics*, Vol. 28 No. 6, pp. 799-807.

Meng, J., Li, Y. and Li, B. (2015), "A dynamic balancing approach for a quadruped robot supported by diagonal legs", *International Journal of Advanced Robotic Systems*, Vol. 12 No. 10.

Polet, D. and Bertram, J. (2019), "A simple model of a quadruped discovers single-foot walking and trotting as energy optimal strategies", BioRXiv.

Pratt, J. and Tedrake, R. (2005), "Velocity based stability margins for fast bipedal walking", Heidelberg.

Raibert, H.M., Blankespoor, K., Nelson, G. and Playter, R. (2008), "BigDog, the Rough-Terrain quadruped robot", *IFAC World COngress*.

Righetti, L. and Ijspeert, A.J. (2008), "Pattern generators with sensory feedback for the control of quadruped locomotion", Pasadena, CA, pp. 819-824.

Skogestad, S.I. (2001), *Multivariable Feedback Control*, John Wiley & Sons, New York, NY.

Sutyasadi, P. and Parnichkun, M. (2016), "Gait tracking control of quadruped robot using differential evolution based structure specified mixed sensitivities H∞ robust control", *Journal of Control Science and Engineering*, Vol. 2016.

Ugurlu, B., Havoutis, I., Semini, C. and Caldwell, D.G. (2013), "Dynamic trot-walking with the hydraulic quadruped robot – HyQ: analytical trajectory generation and active compliance control", *IEEE/RSJ International Conference on Intelligent Robots and Systems* Tokyo.

Wei-Gu, D., Petko, H. and Konstantinov, M.M. (2013), *Robust Control Design with Matlab*, Springer, London.

Zhang, Z.G., Kimura, H. and Fukuoka, Y. (2007), "Self-Stabilizing dynamics for a quadruped robot and extension toward running on rough terrain", *Journal of Robotics and Mechatronics*, Vol. 19 No. 1, pp. 3-12.

Zhang, G. Chai, H. Rong, X. Li, Y. and Li, B. (2014), "An impact recovery approach for quadruped robot with trotting gait", Hailar, s.n., pp. 819-824.

Corresponding author

Petrus Sutyasadi can be contacted at: peter@pmsd.ac.id

Industrial Robot

ORIGINALITY REPORT

16%	12%	11%	%
SIMILARITY INDEX	INTERNET SOURCES	PUBLICATIONS	STUDENT PAPERS

PRIMARY SOURCES

1	www.hindawi.com Internet Source	3%
2	acikerisim.ozal.edu.tr Internet Source	2%
3	Bui Trung Thanh, Manukid Parnichkun. "Balancing Control of Bicyrobo by Particle Swarm Optimization-Based Structure-Specified Mixed H2/H∞ Control", International Journal of Advanced Robotic Systems, 2008 Publication	2%
4	beei.org Internet Source	1%
5	research.ait.ac.th Internet Source	1%
6	Petrus Sutyasadi, Manukid Parnichun. "Trotting control of a quadruped robot using PID-ILC", IECON 2015 - 41st Annual Conference of the IEEE Industrial Electronics Society, 2015 Publication	1%

7	tel.archives-ouvertes.fr Internet Source	1 %
8	Hongbo Zhao. "Construction Schedule Optimization Using Particle Swarm Optimization", 2008 4th International Conference on Wireless Communications Networking and Mobile Computing, 10/2008 Publication	<1 %
9	arxiv.org Internet Source	<1 %
10	researchr.org Internet Source	<1 %
11	Shareef, Zeeshan, Abrar Ahmed, and Naeem Iqbal. "Mixed sensitivity based dynamical Anti-Windup Compensator design using LMI: An application to constrained hot air blower system", 2013 XXIV International Conference on Information Communication and Automation Technologies (ICAT), 2013. Publication	<1 %
12	hdl.handle.net Internet Source	<1 %
13	Parvesh Kumar, Jetesh Raheja. "Optimal design of robust FOPID for the flight control system using multi-objective Differential Evolution", 2015 2nd International Conference	<1 %

	on Recent Advances in Engineering & Computational Sciences (RAECS), 2015 Publication	
14	www.coursehero.com Internet Source	<1 %
15	tutcris.tut.fi Internet Source	<1 %
16	ebin.pub Internet Source	<1 %
17	link.springer.com Internet Source	<1 %
18	shareok.org Internet Source	<1 %
19	www.mdpi.com Internet Source	<1 %
20	Zhang, Xianpeng, Lin Lang, Jian Wang, and Hongxu Ma. "The quadruped robot locomotion based on force control", The 27th Chinese Control and Decision Conference (2015 CCDC), 2015. Publication	<1 %
21	infoscience.epfl.ch Internet Source	<1 %
22	vigir.missouri.edu Internet Source	<1 %

23	hal.archives-ouvertes.fr Internet Source	<1 %
24	Publication	<1 %
25	Sarah Degallier, Ludovic Righetti, Sebastien Gay, Auke Ijspeert. "Toward simple control for complex, autonomous robotic applications: combining discrete and rhythmic motor primitives", Autonomous Robots, 2011 Publication	<1 %
26	Shamel Fahmi, Carlos Mastalli, Michele Focchi, Claudio Semini. "Passive Whole-Body Control for Quadruped Robots: Experimental Validation Over Challenging Terrain", IEEE Robotics and Automation Letters, 2019 Publication	<1 %
27	uwspace.uwaterloo.ca Internet Source	<1 %
28	www.frontiersin.org Internet Source	<1 %
29	www.me.utexas.edu Internet Source	<1 %
30	Moez Davodi, HamidReza Modares, Ehsan Reihani, Mehdi Davodi, Ali Sarikhani. "Coherency approach by hybrid PSO, K-Means clustering method in power system", 2008	<1 %

IEEE 2nd International Power and Energy Conference, 2008
Publication

31	mts.intechopen.com Internet Source	<1 %
32	Yang Zhuo, Guo Li-li, Wan Jian. "Frequency Domain Subspace Decomposition Realization of UWB Synchronization Based on PSO", Information Technology Journal, 2011 Publication	<1 %
33	Zhang, Guoteng, Xuewen Rong, Chai Hui, Yibin Li, and Bin Li. "Torso motion control and toe trajectory generation of a trotting quadruped robot based on virtual model control", Advanced Robotics, 2015. Publication	<1 %

Exclude quotes	On	Exclude matches	< 6 words
Exclude bibliography	On		